energies

Article

Reduction in the Cogging Torques in the DCEFSM Motor by Changing the Geometry of the Rotor Teeth

Andrzej Bień [1], Tomasz Drabek [1,*], Dawid Kara [2] and Tomasz Kołacz [2]

[1] Faculty of Electrical Engineering, Automatics, Computer Science and Biomedical Engineering, AGH University of Science and Technology, 30-059 Krakow, Poland; abien@agh.edu.pl
[2] Department of Electrical Engineering, Polytechnic Faculty, University of Applied Sciences in Tarnow, 33-100 Tarnów, Poland; d_kara@pwsztar.edu.pl (D.K.); tmk@pwsztar.edu.pl (T.K.)
* Correspondence: drabek@agh.edu.pl

Abstract: The paper presents the results of FEM 2D computational studies of a three-phase Direct Current Excited Flux Switching Machine (DCEFSM) electric motor with 15 rotor teeth and 36 stator teeth. The aim of the research was to minimize the cogging torque of the machine by changing the geometry of the rotor teeth and the size of the air gap between the stator and the rotor, with the operating torques unchanged. Computational studies were carried out on the influence of the width of the rotor teeth, the radius of the rounding of their corners, and the size of the air gap on the cogging torque and machine operating torques. The results of the calculations made it possible to select the dimensions of the rotor and the air gap in such a way that the maximum cogging torque was reduced more than six-fold, with the machine operating torques being unchanged. The calculations also showed that it is not possible to increase the value of the operational torques by further changes in the geometry of the rotor teeth and the size of the air gap of the machine.

Keywords: DCEFSM; FEM 2D calculations; electric motor prototype; minimization of the cogging torque

check for updates

Citation: Bień, A.; Drabek, T.; Kara, D.; Kołacz, T. Reduction in the Cogging Torques in the DCEFSM Motor by Changing the Geometry of the Rotor Teeth. *Energies* **2022**, *15*, 2455. https://doi.org/10.3390/en15072455

Academic Editors: Youguang Guo, Gang Lei and Xin Ba

Received: 23 February 2022
Accepted: 25 March 2022
Published: 27 March 2022

1. Introduction

Previous research [1] presented the results of measurements and FEM calculations of a prototype of a three-phase Direct Current Excited Flux Switching Motor (DCEFSM) with 36 stator slots and 15 rotor teeth. The results of measurements and calculations of this motor indicate the necessity to make some structural changes in order to increase the rated torque, reduce the temperature of the windings during rated operation, and reduce the cogging torque of the machine. The problem of reducing the cogging torque in electric machines of various types with radial magnetization has an extensive literature. Typically, it is associated with machines excited by permanent magnets, but cogging torques can also occur in electromagnetically excited machines. The methods of reducing the cogging torque usually do not eliminate it completely. Therefore, a common design practice is to minimize the cogging torque of the machine using more than one reduction method [2–4].

The literature on this subject provides the following methods of reducing the cogging torque in electric machines with radial magnetization:

- choice of the appropriate angular span of magnets in machines excited by permanent magnets [2,5–8];
- making excitation magnets that are skewed [2,5];
- desymmetrization of the arrangement of magnets in the machine [4,9,10];
- choice of the shape of the magnets on the side of the air gap [7];
- making ferromagnetic pole pieces for excitation magnets with an appropriately selected angular span [6];
- construction of a machine with magnets embedded in the rotor ferromagnetic (IPMSM) [7];
- appropriate choice of the angular span of the stator or rotor teeth [11–13];

- appropriate choice of the angular span of the rotor poles (teeth) in reluctance machines [14,15];
- making slots in the stator or rotor that are skewed [3,4,11,14–17];
- desymmetrization of the angular arrangement of rotor poles (teeth) in reluctance machines [4,10,11];
- choice of the shape of the face of the poles/teeth of the stator or rotor [18,19];
- making cuts in the stator teeth or inserting additional teeth [7,15,17];
- using an appropriate current power supply [12,20,21].

The cogging torque is significantly influenced by the size of the air gap between the stator and the rotor [7,8]. The cogging torque decreases as the size of the air gap increases. However, the possibility of reducing the cogging torque by increasing the size of the gap is limited, since this dimension is one of the main dimensions of the machine and is forced by the required value of its rated torque. The rated torque decreases as the gap size increases as it causes the magnetic flux density in the gap to decrease.

The results of extensive research are presented in [15]. A design study of torque pulsation minimization in spoke-type interior permanent magnet motors with a skewed permanent magnet (in different ways) and the notching configurations method has been presented. Notches are dummy slots in either the stator or rotor of the machine. The cogging torque effect of the spoke-type 6S-4P IPM motor design has been investigated and discussed based on 3D FEM calculations. Both methods are effective in not only minimizing the cogging torque, but also in retaining the maximum operating torque.

The original method of limiting the cogging torque is presented in the paper [14]. The paper presents research on the spoke-type interior permanent magnet motor (PMSFM). In order to limit the cogging torque without introducing additional elements to the machine's magnetic circuit and without changing the shape of the magnets, a configuration of the machine with an external rotor was proposed. The use of the external rotor reduced the cogging torque by five-fold and the total torque increased by 8%. The outer rotor machine has 33% less copper weight in the winding, and therefore the power loss in copper was also significantly reduced.

A previous study [12] presented methods of minimizing the torque ripple for the DCEFSM. Based on the harmonics of the self- and mutual inductance of the field and armature windings, it was shown that the sixth harmonic dominates in the torque ripple. It is caused by the sixth harmonic of the self-inductance of the field winding and the fifth harmonic of the mutual inductance between the field winding and the armature winding. A method of minimizing the torque ripple is to add the appropriate harmonic to the armature currents. It has been shown that the additional harmonic content in the armature currents is able to reduce the torque ripple by up to 80%, without reducing the average operating torque.

In [17], two methods of reducing the torque ripple for DCEFSM 12/10 were analyzed. These are: making the rotor with a stepped skew and making non-uniform rotor teeth. The effectiveness of both methods is similar. It was found that saturation had a significant effect on the relationship between the reduction in the torque ripple and the skew angle of the rotor, while the average torque was not changed. Correct selection of the skew angle reduces the torque ripple by at least 50% with a decrease in the average torque of not more than 5%.

The aim of the paper is to present the effect of the dimensions of the rotor teeth of the DCEFSM 36/15 motor and the size of the air gap between the stator and the rotor on the cogging torque of the machine. The practical goal was to select such sizes of the rotor teeth and the air gap so as to minimize the cogging torque of the machine. In this motor, the cogging torque is created by the interaction between the stator teeth and the rotor teeth (poles). The ferromagnetic stator of this motor is typical for an induction motor, and comes from an induction motor rated at 5.5 kW and a synchronous speed of 1500 rpm. It is a 36-slot stator with no skewing of the slots. It was bought as a ready-made induction motor stator (without winding). The 15-tooth rotor was made to order. Therefore, in FEM

2D computational studies, the focus was on limiting the cogging torque by changing the dimensions of the rotor teeth and the air gap between the rotor and stator. The FEM pilot calculations showed that the width of the rotor teeth and the rounding radius of their corners have a significant influence on the cogging torque and the rated torque. Therefore, first, the influence of these dimensions on the cogging torque was determined, and only later was the influence of the air gap size on its value examined. Finally, the peak cogging torque was reduced by more than six-fold, with the rated torque unchanged.

2. Materials and Methods

The calculations were undertaken for the machine with the cross-section shown in Figure 1. The stator outer diameter was 204 mm and the inner diameter was 133.3 mm. The rotor diameter was 132.4 mm. The air gap had a minimum size of 0.475 mm. The length of the stator and rotor was 160 mm. The machine had 36 slots on the stator and 15 teeth on the rotor. In DCEFSM motors, the basic ratio of the number of stator teeth to the number of rotor teeth must be 12:5. Then, the number of pairs of the armature poles is $p_a = 2$, and the excitation is $p_f = 3$. In order to assume a "reasonable" value of the armature supply frequency, which is limited due to the increase in power losses in the ferromagnetic sheets with the increase in this frequency, it was decided to triple these values in order to increase the torque of the machine. This resulted in a machine with 36 stator teeth and 15 rotor teeth. Both the field winding and the phases of the armature had a pitch y = 2. The field winding and the armature winding were made as double-layer windings. The number of pole pairs of the phase was $p_a = 6$, and the number of pole pairs of the field winding was $p_f = 9$, because it was not a rotating field machine. Phases coils were connected in series, and the phases were wye connected. The armature phase coils did not overlap, but they partially overlapped with the coils of the field winding. The coils of the field winding were also connected in series. The motor was powered by sinusoidal three-phase voltages, formed as a function of the measured rotor position. This is a Field Oriented Control (FOC) control system, analogous to the vector control of the speed of PMSM. The operating properties (both static and dynamic) of the motor are analogous to those of a cylindrical synchronous, under-excited and cage-less motor. The rated motor speed of 1500 rpm was achieved with a supply voltage frequency of 375 Hz. The rated motor parameters (obtained from measurements [1]) are presented in Table 1.

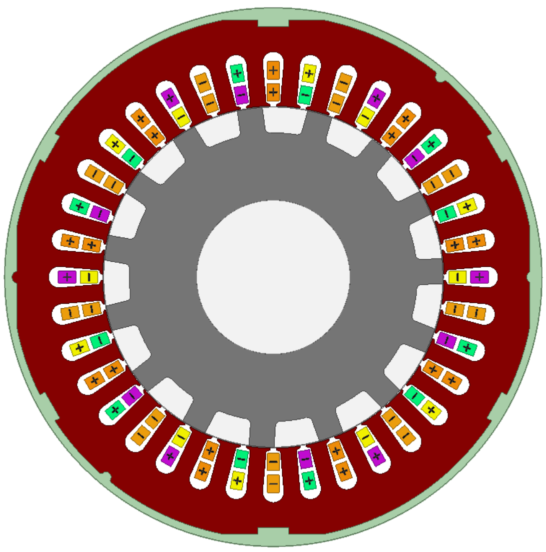

Figure 1. Cross-section of the motor from the model for FEM calculations. Orange color—field winding (for DC current); yellow, green, purple—phase windings (for AC currents); red, grey—ferromagnetic sheets of the stator and rotor.

Table 1. Rated motor parameters.

Motor Parameter	Value	Comment
Power (on the shaft)	3.5 kW	at speed 1500 rpm
Armature Power	4.03 kW	at speed 1500 rpm
Field Winding Power	0.25 kW	at field current 9 A
Rotation Speed	1500 rpm	at frequency 375 Hz and voltage 475 V
Frequency	375 Hz	at speed 1500 rpm
Voltage (phase-to-phase RMS)	475 V	at speed 1500 rpm
Torque	22.3 Nm	thermally limited
Armature Current (RMS)	7.45 A	thermally limited value at speed 1200 rpm
Field Current (DC)	9 A	thermally limited value at speed 1200 rpm

The rated values of both currents result from the admissible temperature of both windings during their operation (due to the thermal class of their insulation). According to the results of the FEM calculations, in motors of this type, the torque increases linearly with the armature current to the RMS values of the current of 9 A. The RMS value of the armature current of 7.45 A is only due to the thermal limitation. Increasing the armature current results in a further increase in the machine torque, although this increase is not linear. Then the rated torque of the motor would also be twice as large. The situation regarding the field current is different, the increase of which above the value of approx. 10 A results in only a slight increase in the machine torque due to the saturation of the excitation magnetic circuit. The assumed nominal value of 9 A, due to the thermal limitation, is not much lower than 10 A. Compared to 10 A, it results in torque that is only about 5% lower (for a set armature current). The measurements, the results of which are presented in a previous paper [1], were made at the speed of 1200 rpm, instead of the rated speed of 1500 rpm, due to technical limitations on the test bench. Therefore, the calculations in this paper were also carried out at a speed of 1200 rpm, for the sake of consistency with the earlier paper [1]. The results of the FEM 3D calculations performed at that time (taking into account the power losses in ferromagnetic sheets) show that the results of the FEM 2D calculations obtained for the speed of 1200 rpm can be extrapolated to the speed of 1500 rpm. According to the earlier FEM 3D calculations, the increase in power losses in sheets with the increase in the rotation speed from 1200 to 1500 rpm did not affect the average machine torque value or the peak value of the cogging torque. Of course, the efficiency of the motor decreases due to the losses in ferromagnetic sheets.

To determine the appropriate dimensions of the rotor teeth, 4 criteria were taken into account:

1. Minimizing the amplitude of the pulsation of the total machine torque;
2. Minimization of the maximum value of the cogging torque and obtaining a smooth curve of it as a function of the rotor position (i.e., minimization of the derivative value $dT_c/d\phi$);
3. Obtaining the value of the maximum motor starting torque not lower than 95% of its current maximum value;
4. Obtaining the value of the rated torque of the motor not lower than 95% of its current value.

Two coefficients were introduced to quantify the fulfillment of criteria 1 and 2. The first is the pulsation coefficient of the total electromagnetic torque of the motor:

$$\varepsilon = \frac{\max(T_e) - \min(T_e)}{\mathrm{mean}(T_e)} \cdot 100\% \tag{1}$$

The second factor is the cogging torque content in the electromagnetic torque of the motor:

$$\tau = \frac{\max(T_c)}{\max(T_e)} \cdot 100\% \tag{2}$$

FEM 2D calculations of the machine cross-section with a stopped or rotating rotor were performed, taking into account non-linear magnetization of stator and rotor sheets. The hysteresis loop of the magnetization characteristic of the sheets and the power losses in the sheets were not taken into account. In calculations, the stator phases were powered by sinusoidal alternating currents, with sinusoids formed as a function of the rotor position (as in the Field Oriented Control of this motor), or the phases were powered by constant currents with values corresponding to the selected time moment of the three-phase sinusoidal waveforms of currents.

The torque (as the electromagnetic torque of the machine) was calculated with the rotor rotating at a set speed and with the AC (three-phase armature, sinus) and DC (field winding) current supply of the motor windings. The starting torque and the cogging torque were calculated for the stopped rotor, for successive rotor positions, and with the DC current supply (armature winding and field winding or only field winding for the cogging torque). T_s is the mean starting torque. The values of the currents in each phase correspond to the selected moment of the three-phase AC system.

3. Results

3.1. Rotor with Original Teeth (Model A)

Figure 2 shows the rotor tooth shape of the existing machine from Figure 1 (as Model A). This motor was made as a prototype motor by ATB Tamel (Poland).

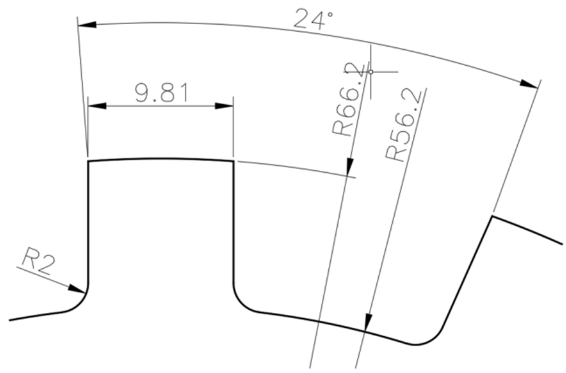

Figure 2. Machine rotor tooth shape, Model A.

The cogging torque T_c was calculated with a stopped rotor for the field current of 8 A (DC) and the zero armature current. The operating torque of the motor was obtained for the same value of the field current with a rotating rotor at the speed of 1000 rpm and for the three-phase, sinusoidal supply of the armature phases with currents having an RMS value of 6.9 A and a frequency of 250 Hz. The static starting torque T_s was obtained with a stopped rotor from the calculations for supplying the two phases of the armature with direct current, respectively +8.5 A and −8.5 A, and the field current 8 A. Figure 3 shows the obtained angular waveforms for these supply conditions. Table 2 summarizes the values of torques and the coefficients ε and τ. These waveforms and values are a reference for the calculation results obtained for changing tooth widths, the radii for rounding their corners, and the size of the air gap.

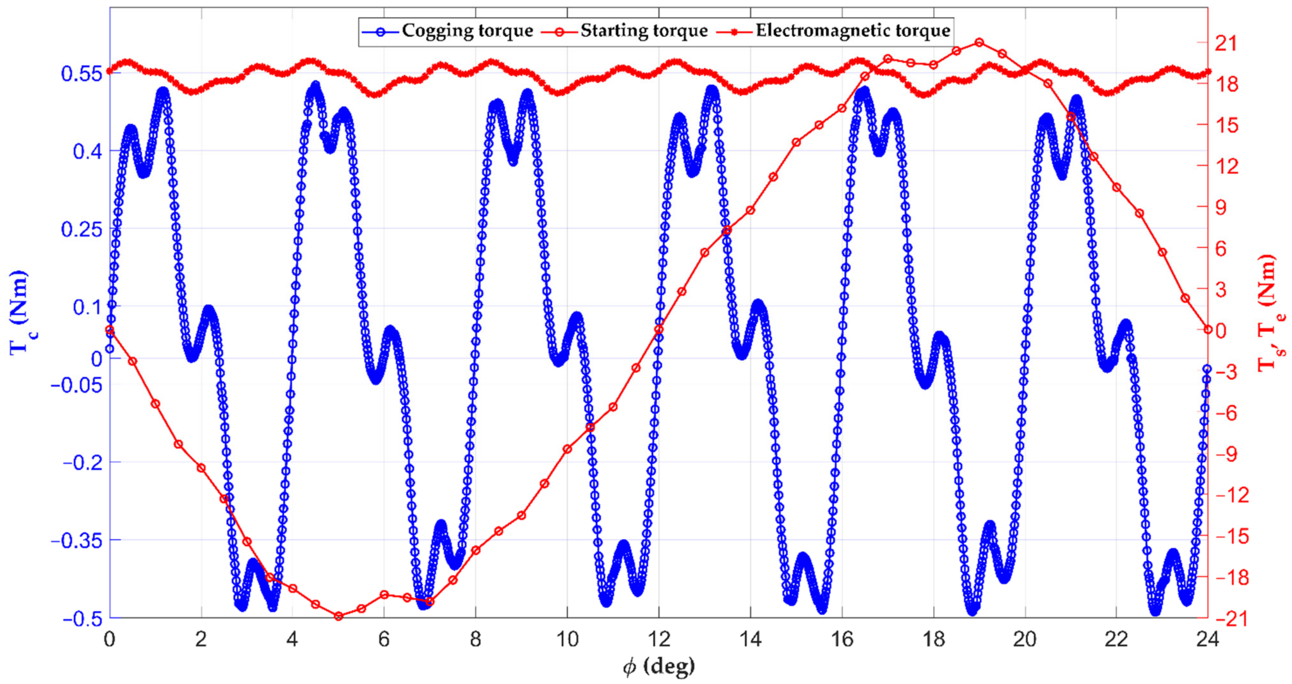

Figure 3. Cogging, starting, and operating torque as a function of the rotor angle of the existing machine, Model A.

Table 2. Summary of the calculation results of Model A.

Rotor Tooth Dimensions		T_c [Nm]	T_s [Nm]	T_e [Nm]			ε [%]	τ [%]
s_z [mm]	r_z [mm]	Max	Max	Min	Avg	Max		
9.81	0	0.53	20.88	17.13	18.54	19.63	13.48	2.7

3.2. Rotor with Changed Tooth Width and Tooth Corners Radius (Model B)

For Model B (Figure 4), the variable parameters, on which the value of the cogging torque depends, were: tooth width s_z varied in the range from 5 to 20 mm with step 0.5 mm, and the tooth corner rounding radius r_z varied in the range from 0 to 3.5 mm with step 0.5 mm. The other machine dimensions remained unchanged in reference to Model A. The current and velocity conditions for determining the torques were identical as for Model A.

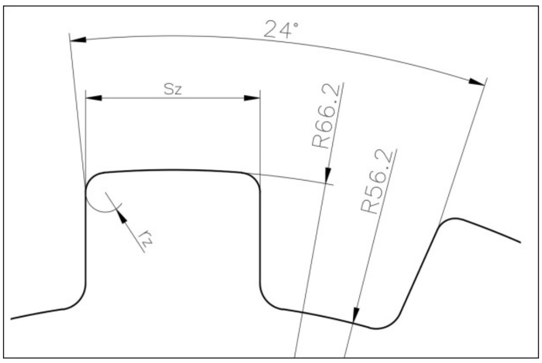

Figure 4. Machine rotor tooth shape, Model B.

As can be seen from Figure 5, the local minimums of the maximum cogging torque occur for each radius r_z. The analysis of the obtained distributions shows that the most advantageous modification of the rotor would be to change the width of the teeth to

s_z = 8 mm and the radius of rounding of their corners to r_z = 1 mm. This guarantees a minimum value of maximum cogging torque. Very similar values were also obtained for two other tooth widths: s_z = 12.5 mm and s_z = 17 mm, with the same corner rounding radius r_z = 1 mm.

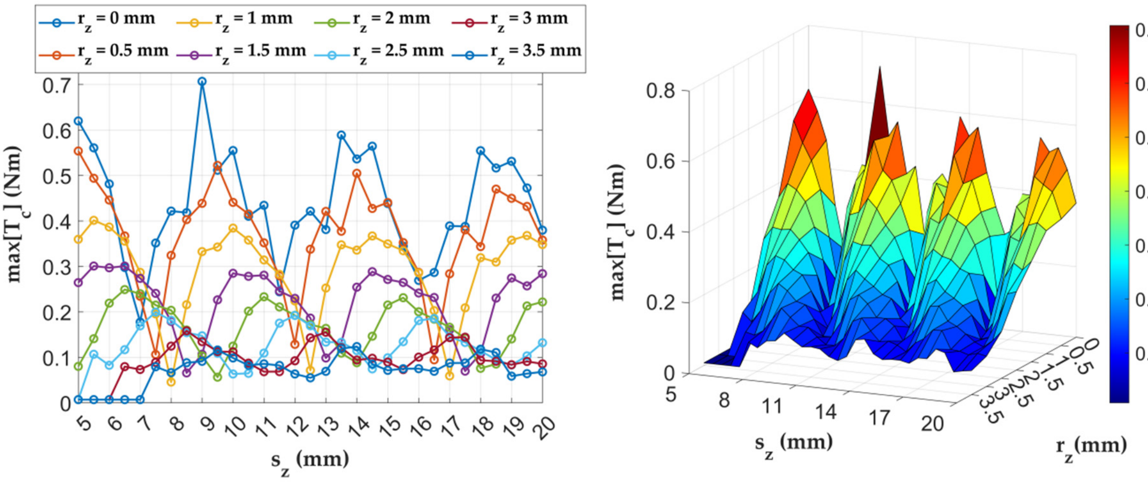

Figure 5. Relationship of the maximum cogging torque to the width of the rotor teeth and the radius of rounding of their corners.

Table 3 shows the smallest values of the maximum cogging torque for each tested rotor teeth corner radius.

Table 3. List of the minimum values of the maximum cogging torque as a function of the radius of rounding of the teeth corners.

No.	Rotor Tooth Dimensions		T_c [Nm]
	s_z [mm]	r_z [mm]	Max
1	7	0	0.1777
2	7.5 and 16.5	0.5	0.0947
3	8	1	0.0458
4	8.5	1.5	0.0659
5	9.5	2	0.0566
6	10	2.5	0.0636
7	11	3	0.0686
8	12.5	3.5	0.0551

Figure 6 shows the maximum starting torque of the motor as a function of the width of the teeth and the radius of rounding of their corners. The static characteristic of the starting torque as a function of the rotor position angle was determined for each combination of the variables s_z and r_z, with the rotor stopped and the supply of two armature phases, and the field winding as in the analogous calculations of Model A. It can be seen that the relationship between the starting torque and the dimension s_z has one maximum global. Its value is 22.5 Nm with a tooth width of 12.5 mm and no tooth rounding (r_z = 0 mm).

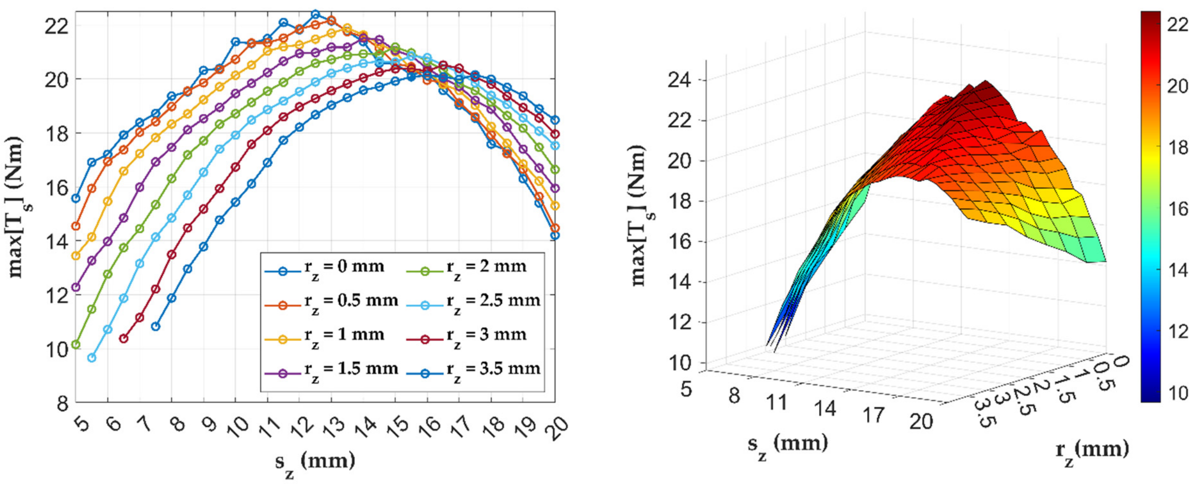

Figure 6. Maximum starting torque as a function of the width and radius of the rounding of the rotor teeth.

Figure 7 shows the change in the average operating torque of the motor as a function of the width of the teeth and the radius of the rounding of their corners. The dependence of the operating torque on the rotor position angle was determined for each combination of the variables s_z and r_z and for the value of sinusoidal phase currents of 6.9 A (RMS). The average electromagnetic torque (for one rotation of the rotor) reached the maximum value of 18.6 Nm for various configurations of the tested dimensions of the rotor tooth.

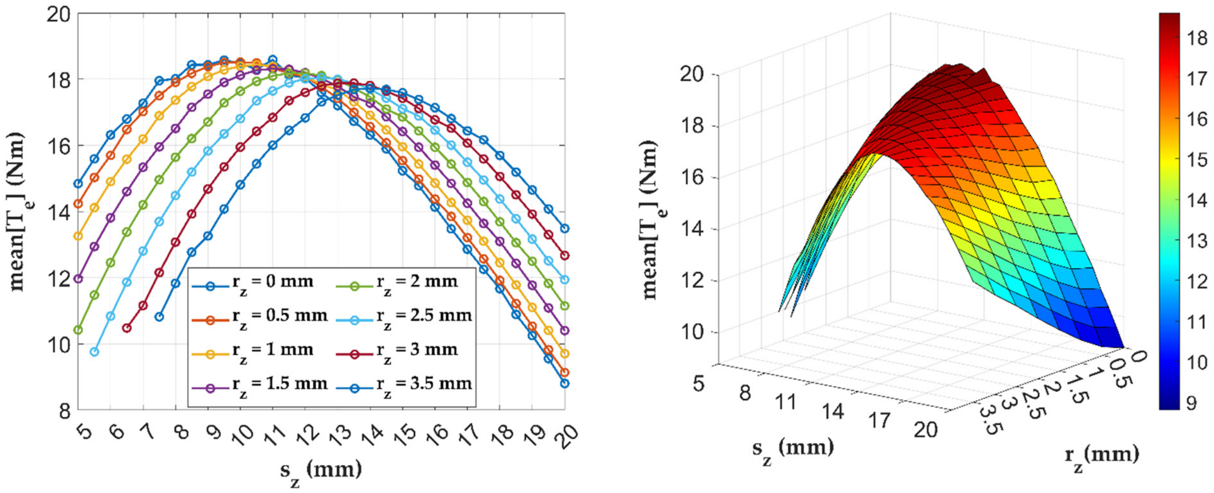

Figure 7. Average operating torque as a function of the width and radius of the rounding of the rotor teeth.

Table 4 shows the maximum values of the maximum starting torque and average operating torque for each of the rotor teeth corner rounding radii r_z. The greatest values of both torques were provided by the tooth width s_z = 12.5 mm and the rounding radius r_z = 0 mm, and were 107% and 100%, respectively, of that of Model A. It can be seen that the negative impact of rounding the tooth corners on the value of both torques becomes visible only at high values of r_z > 1.5 mm. Up to a value of r_z = 1.5 mm, both torques hardly depend on the r_z value.

Table 4. Summary of the maximum values of the starting torque and the average values of the operating torque as a function of the radius of the rounding of the tooth corners.

No.	Rotor Tooth Dimensions		T_s [Nm]	T_e [Nm]
	s_z [mm]	r_z [mm]	Max	Avg
1	12.5	0	22.3956	18.5895
2	13	0.5	22.1735	18.5151
3	13.5	1	21.8866	18.4349
4	14	1.5	21.5116	18.3147
5	15	2	21.1775	18.1838
6	15.5	2.5	20.8483	18.0441
7	16.5	3	20.5114	17.8801
8	17.5	3.5	20.1541	17.7249

Figure 8 shows the dependence of the torque pulsation ε and the cogging torque content factor τ on the parameters s_z and r_z.

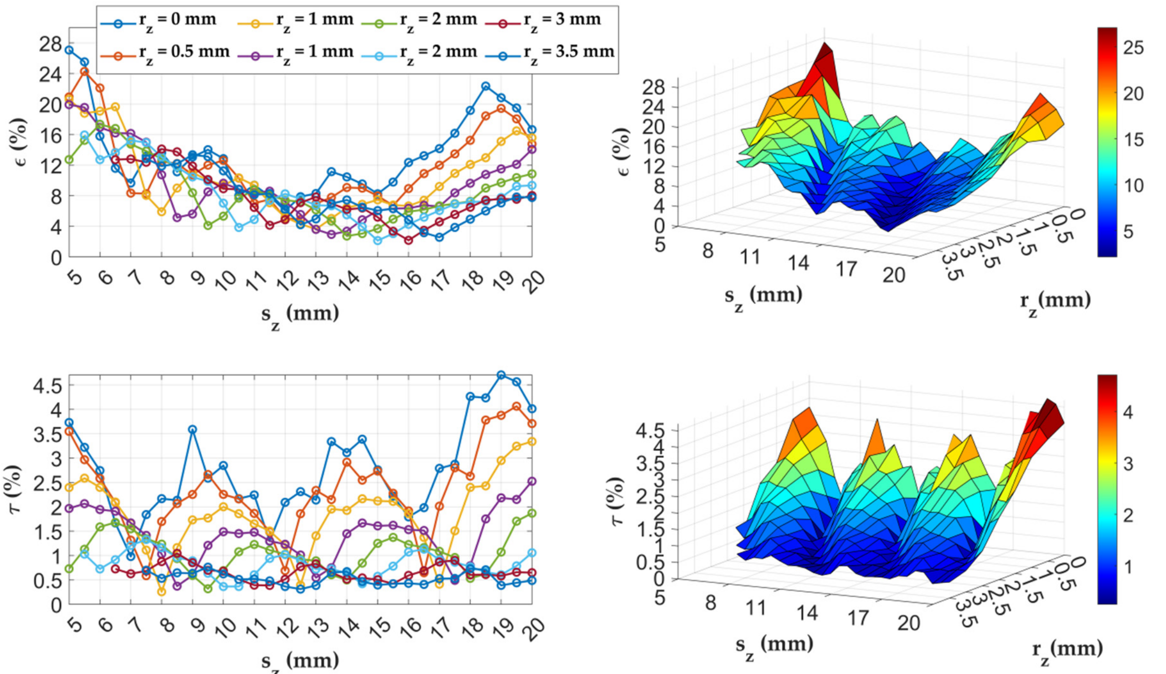

Figure 8. The torque pulsation factor ε and the cogging torque content factor τ as a function of the width and corner radius of the rotor tooth.

For each radius r_z, the smallest values of the coefficients ε and τ as a function of the dimension s_z were selected and are presented in Table 5.

Figure 8 and Table 5 show that the pulsation of the torque ε is the smallest for the width of the teeth s_z = 15 mm and the radius of rounding of their corners r_z = 2.5 mm. The coefficient τ is the smallest for teeth with a width of s_z = 8 mm and a corner rounding radius r_z = 1 mm.

After taking into account the dependence from Figures 6–8 in the context of the adopted optimization criteria, the area of variability in the width of the rotor teeth, which was subjected to further tests, was limited to the range from s_z = 10 to 16 mm. The step for changing the width in the FEM calculations was reduced to 0.1 mm to increase the accuracy of the calculations and to be closer to the ideal solution meeting the adopted criteria. The range of variability in the radius of the rounding of the tooth corners did not change ($r_z = 0 \ldots 3.5$ mm).

Table 5. List of the smallest values of the ε and τ coefficients.

No.	Rotor Tooth Dimensions		ε [%]	Rotor Tooth Dimensions		τ [%]
	s_z [mm]	r_z [mm]	Min	s_z [mm]	r_z [mm]	Min
1	12	0	6.0634	7	0	0.9810
2	12.5	0.5	4.8921	7.5	0.5	0.5871
3	13	1	3.6321	8	1	0.2573
4	13.5	1.5	2.9448	8.5	1.5	0.3732
5	14	2	2.7315	9.5	2	0.3295
6	15	2.5	2.1374	10	2.5	0.3645
7	16	3	2.1706	11.5	3	0.3873
8	17	3.5	2.5680	12.5	3.5	0.3117

The most favorable results for the adopted criteria were selected from Figures 9–12 and are presented in Table 6.

Table 6 summarizes the results of the calculations that meet the adopted criteria for optimizing the dimensions of the rotor. The smallest value of the cogging torque occurs for the tooth width s_z = 12.8 mm and their rounding radius r_z = 3.5 mm. These dimensions, however, are not satisfactory due to the decrease in the value of the starting torque of the motor (18.9 vs. 20.88 Nm in Model A). The main goal of the optimization was to reduce the cogging torque, but with the condition of maintaining the motor torques (maximum starting torque and average operating torque) at a minimum of 95% of their level. Therefore, the final design parameters of the Model B rotor were the tooth width s_z = 13.3 mm and the corner rounding radius r_z = 1.5 mm. With these dimensions, the maximum cogging torque decreased to 0.079 Nm, i.e., 85% compared to Model A. The maximum starting torque increased minimally, to 21.2 Nm, i.e., by 1.6% compared to Model A. The average operating torque decreased to 17.6 Nm, i.e., by 5.1%. Comparison of the torques of Models A and B (with the final design parameters) as a function of the angle of the rotor position is shown in Figure 13.

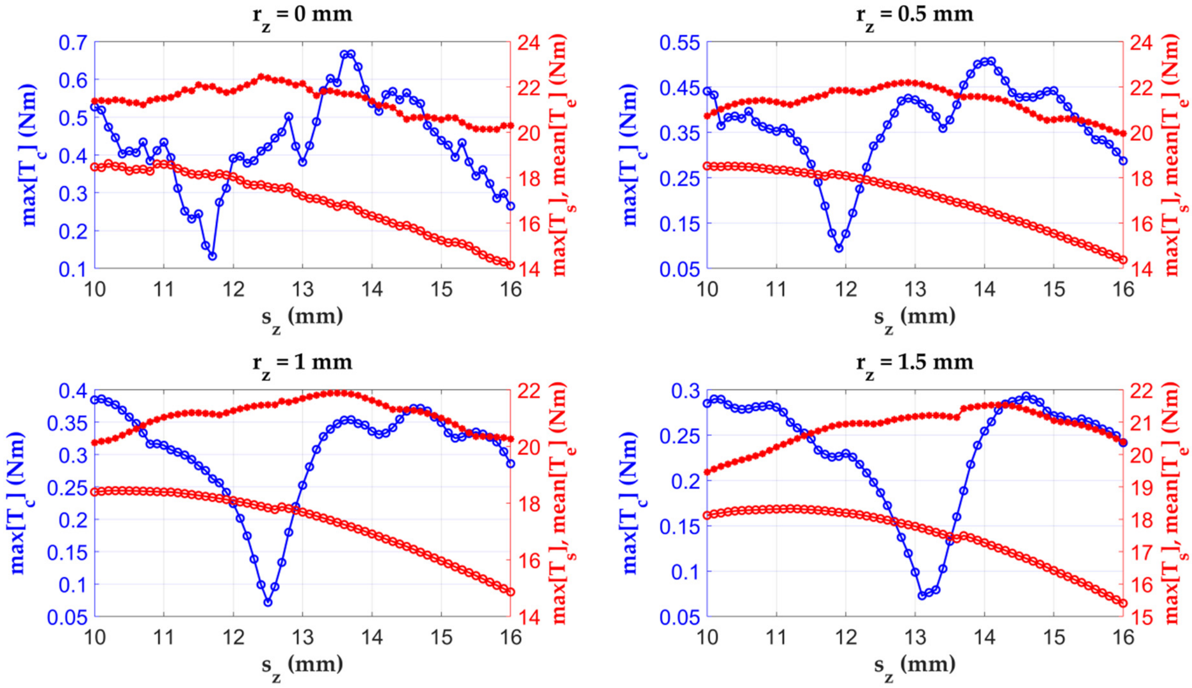

Figure 9. Values of the maximum cogging torque, maximum starting torque, and average operation torque as a function of the width of the teeth for different radii of the rounding of their corners ($r_z \in <0$, 1.5 mm $>$).

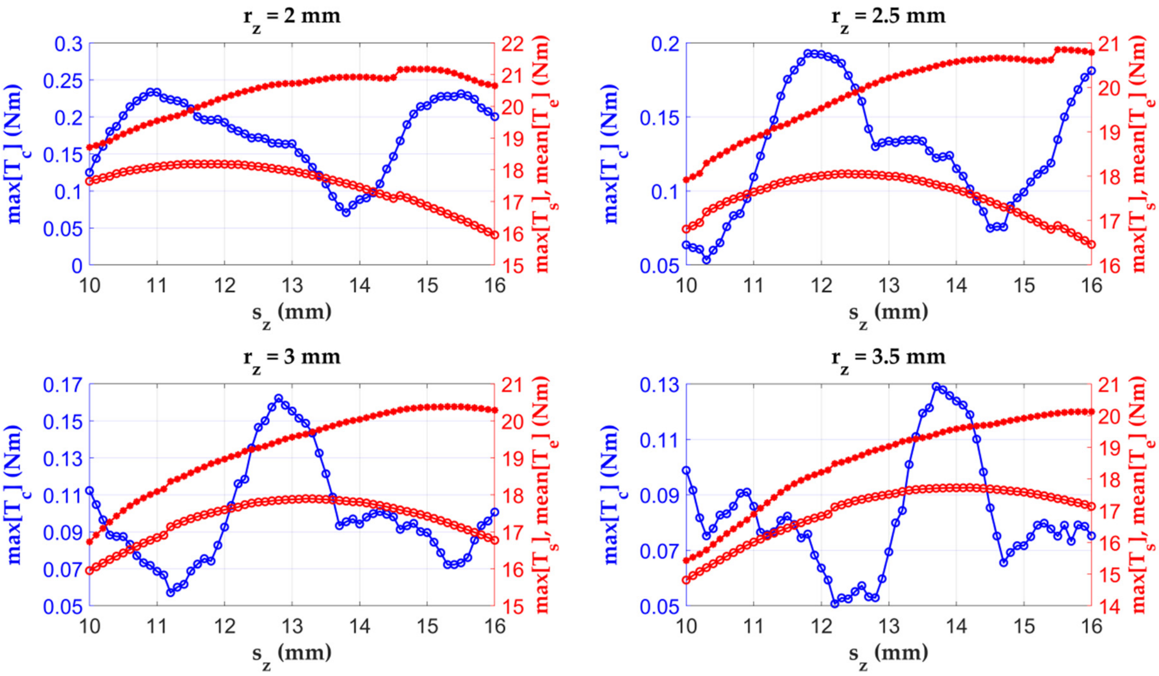

Figure 10. Values of the maximum cogging torque, maximum starting torque, and average operation torque as a function of the width of the teeth for different radii of the rounding of their corners ($r_z \in < 2,\ 3.5\ \text{mm} >$).

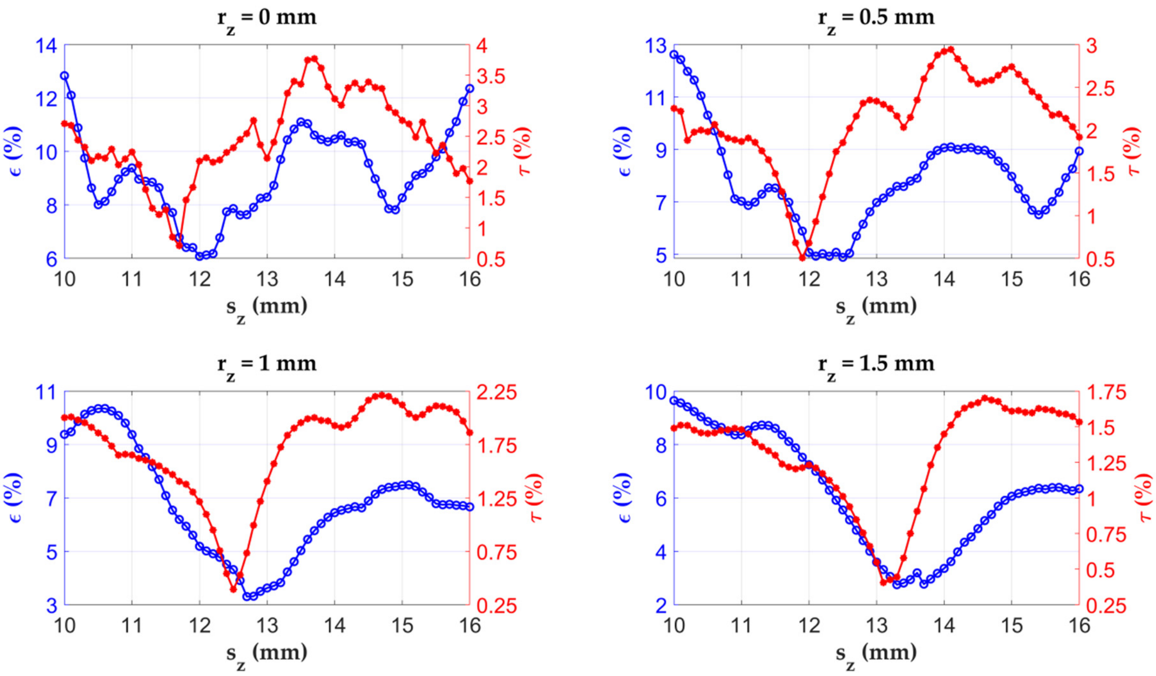

Figure 11. The coefficient of pulsation of the operation torque and the coefficient of the cogging torque content in the operation torque, as a function of the width of the teeth, for different radii of the rounding of their corners ($r_z \in < 0,\ 1.5\ \text{mm} >$).

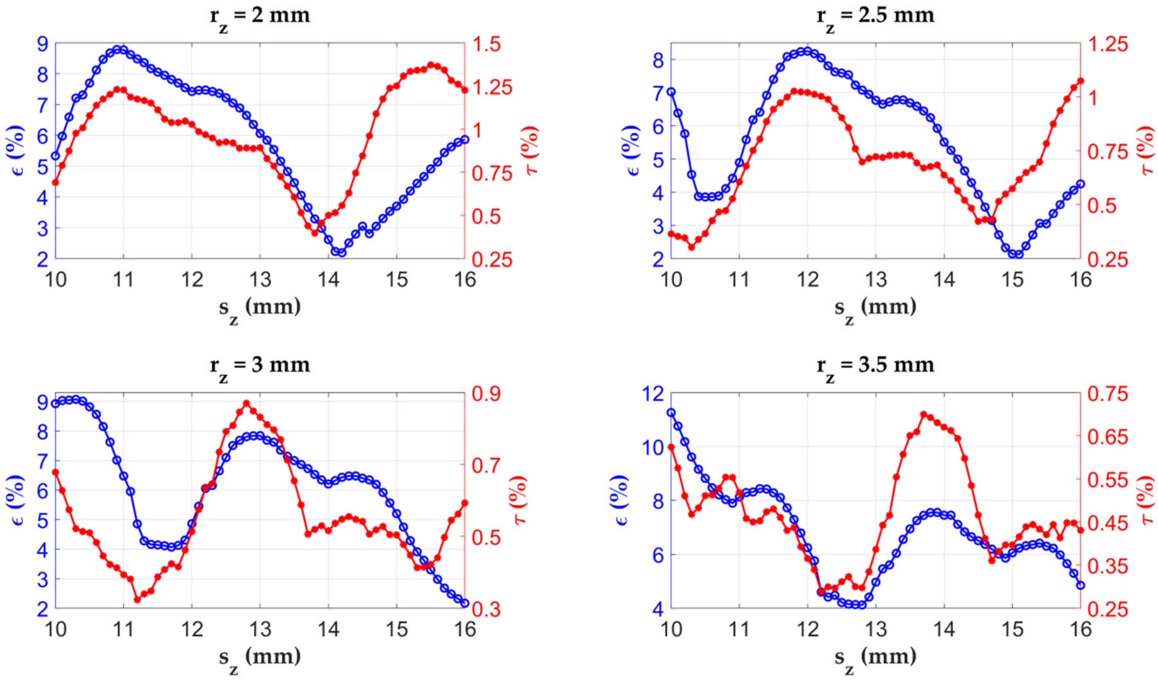

Figure 12. The coefficient of pulsation of the operation torque and the coefficient of the cogging torque content in the operation torque, as a function of the width of the teeth, for different radii of the rounding of their corners ($r_z \in < 2,\ 3.5\ \text{mm} >$).

Table 6. Summary of the calculation results for various dimensions of the rotor teeth.

No.	Rotor Tooth Dimensions		T_c [Nm]	T_s [Nm]	T_e [Nm]			ε [%]	τ [%]
	s_z [mm]	r_z [mm]	Max	Max	Min	Avg	Max		
1	11.7	0	0.13	22.03	17.53	18.06	18.75	6.78	0.71
2	11.9	0.5	0.095	21.86	17.63	18.12	18.71	5.89	0.51
3	12.5	1	0.072	21.47	17.45	17.83	18.22	4.32	0.39
4	13.1	1.5	0.073	21.19	17.38	17.72	17.97	3.32	0.41
5	13.2	1.5	0.076	21.21	17.37	17.66	17.91	3.1	0.43
6	13.3	1.5	0.079	21.21	17.35	17.6	17.84	2.75	0.45
7	13.8	2	0.071	20.92	17.25	17.56	17.82	3.28	0.39
8	14.1	2	0.091	20.92	17.17	17.38	17.55	2.23	0.52
9	14.5	2.5	0.075	20.65	17.03	17.43	17.72	3.39	0.42
10	14.7	2.5	0.076	20.66	17.00	17.3	17.55	3.15	0.43
11	10.3	2.5	0.053	18.3	16.89	17.19	17.67	4.53	0.3
12	10.4	2.5	0.06	18.39	17.05	17.27	17.72	3.87	0.34
13	11.2	3	0.057	18.4	16.80	17.14	17.64	4.84	0.32
14	11.8	3	0.074	18.84	17.15	17.51	17.87	4.13	0.42
15	15.3	3	0.072	20.4	16.83	17.24	17.50	3.91	0.41
16	15.6	3	0.076	20.37	16.77	17.05	17.28	2.98	0.44
17	12.2	3.5	0.051	18.48	16.81	17.12	17.60	4.6	0.29
18	12.8	3.5	0.053	18.9	17.05	17.44	17.77	4.12	0.3
19	14.7	3.5	0.066	19.8	17.09	17.56	18.19	6.19	0.36
20	15.7	3.5	0.073	20.16	16.69	17.3	17.72	5.98	0.41

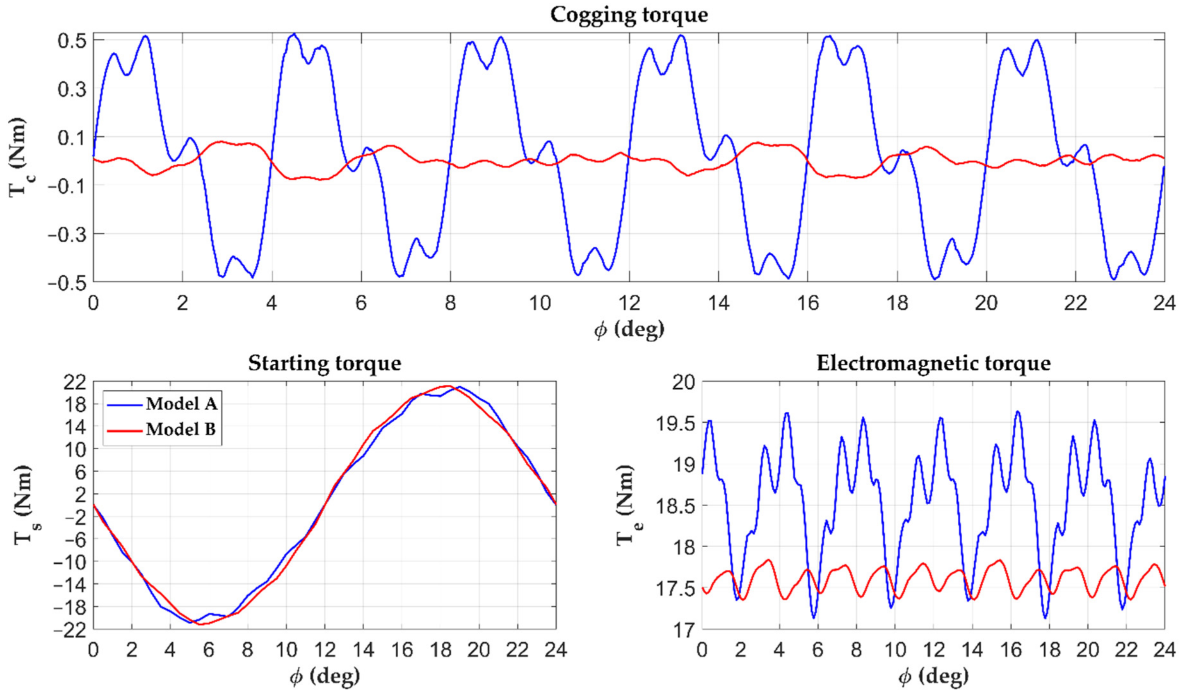

Figure 13. Comparison of the torques of Models A and B as a function of the angle of the rotor position.

3.3. *Influence of the Air Gap Size on the Cogging Torque*

The size of the air gap has a great effect on the cogging torque of electric machines and their operational torques [7,8]. Figure 14 shows the dependence of the three torques—maximum cogging torque, maximum starting torque, and average operating torque—and the coefficients ε and τ on the size of the air gap. These relationships are for Model B (s_z = 13.3 mm, r_z = 1.5 mm).

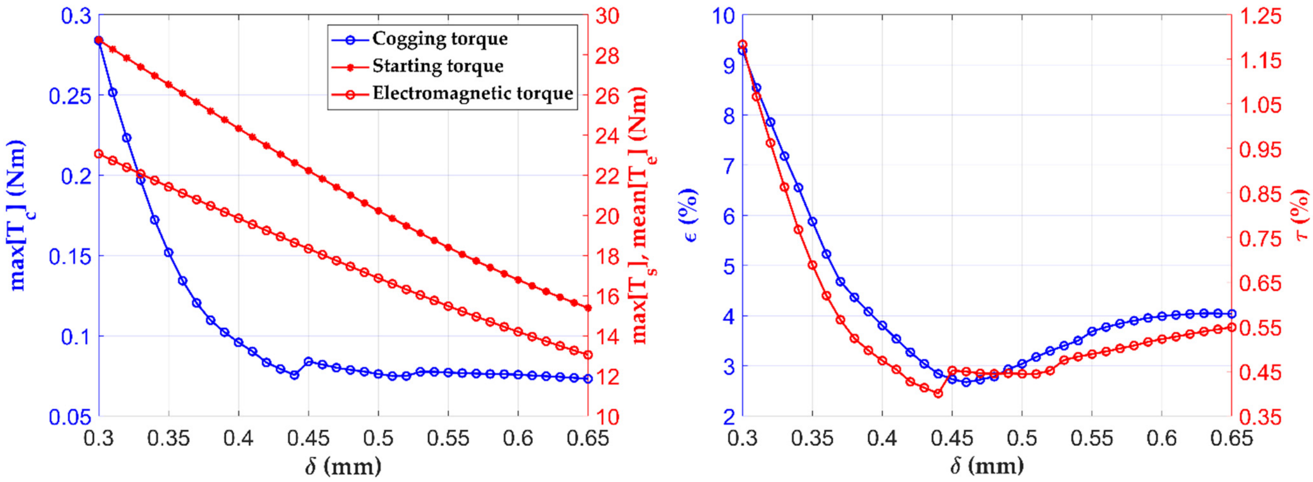

Figure 14. Relationships of the motor torques and the ε and τ coefficients to the size of the air gap.

The calculation results presented in Figure 14 show that increasing the air gap causes a decrease in the value of the maximum cogging torque and the coefficients ε and τ. Unfortunately, the values of the operational torques also decrease. Increasing the size of the air gap above approx. 0.42 mm does not result in significant changes in the maximum value of the cogging torque and both coefficients, but it causes a further decrease in the value of the operating torques. This is caused by the decrease in the value of the magnetic flux density in the air gap, with the supply of the motor windings with currents. On this basis, for Model C of the motor, the final dimension of the air gap $\delta = 0.42$ mm was selected, with the dimensions s_z and r_z as for Model B.

Figure 15 shows the angular waveforms of torques of all three models. The numerical results of the optimization of the rotor dimensions for all three models are summarized in Table 7.

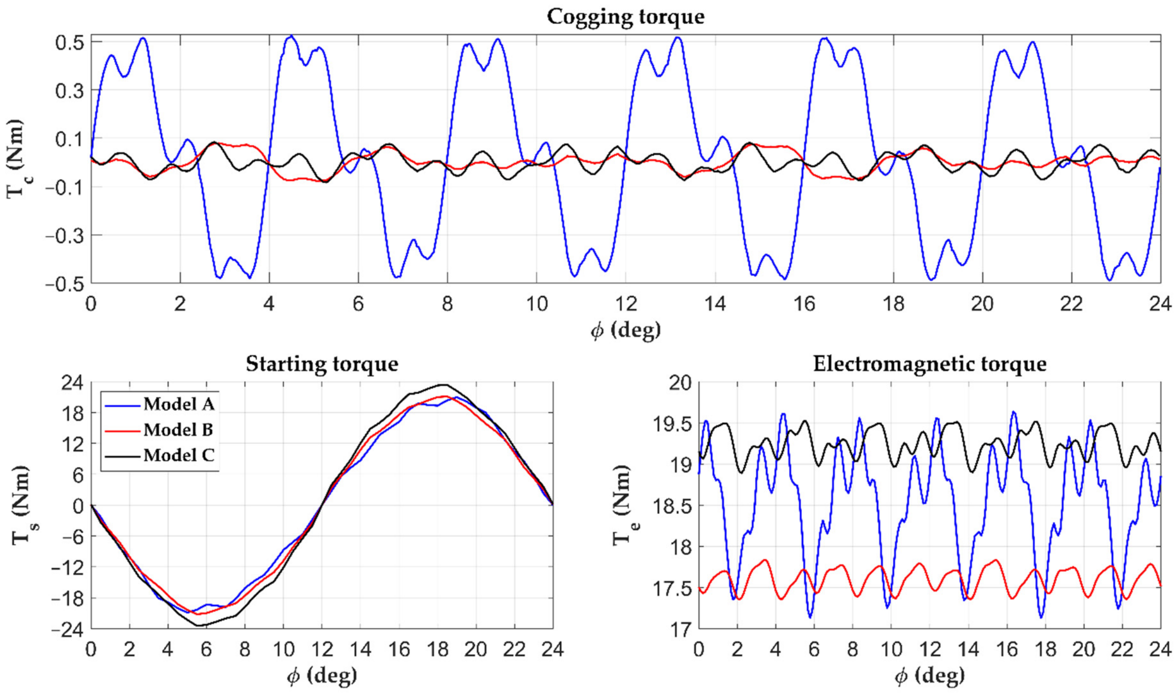

Figure 15. Comparison of the torques of Models A, B, and C as a function of the angle of the rotor position.

Table 7. Summary of the calculation results of Models A, B, C.

Rotor	Rotor Dimensions			T_c [Nm]	T_s [Nm]	T_e [Nm]	ε [%]	τ [%]
	s_z [mm]	r_z [mm]	δ [mm]	Max	Max	Avg		
Model A	9.81	0	0.475	0.53	20.88	18.54	13.48	2.7
Model B	13.3	1.5	0.475	0.079	21.21	17.6	2.75	0.45
Model C	13.3	1.5	0.42	0.083	23.47	19.24	3.27	0.43

4. Discussion

Figure 5 shows that the magnitude of the maximum cogging torque depends on the relationship of the rotor tooth width to the stator tooth width. When $r_z = 0$ mm, the maximum cogging torque reaches the greatest values with the width of the rotor tooth being half the width of the stator tooth ($s_z = 1, 2, 3, \ldots \cdot \frac{1}{2} s_z$ of the stator). Figure 5 also shows that the rounding of the corners of the rotor teeth has a significant influence on the magnitude of the maximum cogging torque. It decreases monotonically with the increase in the radius of this rounding, for each width of the rotor teeth. At the same time, an increase in the value of r_z causes an increase in the value of s_z, where the local maximum cogging torque occurs.

The maximum starting torque and average operating torque achieve their greatest values for the width of the rotor teeth greater than $s_z = 9.81$ mm from Model A: $s_z = 10 \ldots 16$ mm, depending on the size of the corner rounding radius r_z (Figures 6 and 7). An increase in the value of r_z causes an increase in the required value of s_z, which guarantees the highest values of both torques. With $r_z = 0$ mm (as in Model A with $s_z = 9.81$ mm), the greatest values of both torques occur, respectively, of $s_z = 12.5$ mm and $s_z = 9 \ldots 11$ mm.

With r_z= 1.5 mm (as in the Model C), the greatest values of both torques occur, respectively, of s_z= 14 . . . 14.5 mm and s_z= 10.5 . . . 12 mm.

The values of the ε coefficient in Figure 8 reach their minima at the width of the rotor teeth s_z= 12 . . . 13 mm, for all values of the radius r_z. The coefficient τ reaches its maximums for those values of the width s_z for which the maximum cogging torque is the greatest. The minima of the values of τ occur for those values of s_z for which the maximum cogging torque is the smallest.

Figures 9 and 10 show that with the increase in the radius of the rounding of the rotor teeth corners, the minimum value of the maximum cogging torque shifts in the direction of the increase in the width of the teeth—from s_z = 11.7 mm for r_z = 0 mm to s_z = 13.8 mm for r_z = 2 mm. The change in the shape of the dependence of the value of the maximum cogging torque on the width of the teeth, as a function of r_z, at a value of r_z = 2.5 mm, results in a new minimum of this torque, of s_z = 10.3 mm. With further increases in the radius r_z, the minimum also shifts in the direction of increasing the value of s_z; for r_z = 3.5 mm it reaches s_z = 12.2 mm. Although the shape of the dependence of the value of the maximum cogging torque on the width of the teeth s_z changes with the change in the value r_z, its general character is retained. This can be considered to be an indirect confirmation of the correctness of the FEM calculations.

As the radius of the tooth corner rounding rises, the minimum value of the ε coefficient also shifts in the direction of the tooth width increase (Figures 11 and 12). Contrary to the value of the maximum cogging torque, this occurs in the full range of radius r_z changes, because the new minimum value of ε, appearing at the value r_z = 2.5 mm, has a lower value than the “old” minimum. Both minimums are shifting towards an increase in the value of s_z. The shape of the relationship $\varepsilon(s_z)$ changes smoothly with the change in the value of r_z, which can be considered to be an indirect confirmation of the correctness of the FEM calculations.

The minimum value of the coefficient τ from Figures 11 and 12 behaves similarly—as the radius r_z increases, it moves towards the increase in the value of s_z. With r_z = 2.5 mm, a new minimum τ appears, unlike for ε, with a lower value of τ than with the “old” minimum. The shape of the relationship $\tau(s_z)$ changes smoothly with the change in the value r_z, which is also an indirect confirmation of the correctness of the FEM calculations.

The increase in the size of the air gap δ (Figure 14) causes a decrease in the values of all three torques of the motor and the coefficients ε and τ. The decrease in the value of the torques is due to the decrease in the magnetic flux density in the machine air gap with the increase in its dimension, due to the current supply of the motor windings. However, the decrease in the value of the maximum cogging torque is not linear, which made it possible to determine the size of the air gap, above which this torque practically does not decrease. This size was fixed for the final machine Model C. This size is a little smaller than that in Model A (0.42 vs. 0.475 mm).

The test results confirmed the thesis that it is possible to significantly reduce the value of the cogging torque in the DCEFSM machine without reducing the value of its average torques. In the final Model C, there was even a certain increase in the value of torques—maximum starting torque increased by 12% and average operating torque by 3.7%. The goal of minimizing the cogging torque was achieved despite a certain reduction in the dimension of the air gap in relation to Model A. The research also showed that to minimize the cogging torque it is not necessary to modify the stator sheets, which is important for practical reasons. The high dimensional resolution of the FEM calculations made it possible to accurately determine the variability in the machine torques and the values of the coefficients ε and τ with the dimensions s_z, r_z, and δ. Rounding the corners of the rotor teeth forced a significant compaction of the FEM mesh around these corners, especially on the side of the air gap. The problem of the accuracy of FEM calculations near the edge is known in the literature. Incorrect selection of the number of finite elements or their shape near the edges can lead to significant errors in FEM calculations [8].

5. Conclusions

The research carried out resulted in the following conclusions:

1. It is possible to significantly (more than six-fold) limit the maximum value of the cogging torque in the DCEFSM motor only by changing the geometry of the rotor teeth and the size of the air gap. This does not reduce the operating torque and starting torque of the motor.
2. Rounding the corners of the rotor teeth, which is generally not practiced in electrical machines, has a significant impact on the cogging torque. It also helps to reduce the value of the $dT_c/d\phi$ derivative, which affects the smoothness of the rotor movement during rated motor operation.
3. The dependence of the cogging torque on the size of the air gap is non-linear, i.e., with saturation. This made it possible to select the correct size of the air gap, guaranteeing the minimization of the cogging torque while maintaining the values of the operating and starting torques.
4. Calculations showed that it is not possible to further increase the operating torque of the machine by changing the geometry of the rotor teeth and the size of the air gap. The operating torque can be increased only by increasing the value of the field current and/or the armature current. Unfortunately, this will require enlarging the stator slots, for the field winding and/or for the armature winding.

Author Contributions: Methodology, A.B., T.D. and D.K.; software, D.K. and T.K.; formal analysis, A.B., T.D. and T.K.; resources, T.D. and D.K.; data curation, D.K. and T.K.; writing—original draft preparation, T.D. and D.K.; writing—review and editing, A.B., T.D. and T.K.; visualization, D.K. and T.K.; supervision, T.D., T.K. and D.K. All authors have read and agreed to the published version of the manuscript.

Funding: This research was funded by University of Applied Sciences in Tarnow, grant number PWSZ/PRNR-s/0700-11/PN-U/2021.

Institutional Review Board Statement: Not applicable.

Informed Consent Statement: Not applicable.

Data Availability Statement: The data presented in this study are available on request from the corresponding author.

Conflicts of Interest: The authors declare no conflict of interest.

References

1. Drabek, T.; Kara, D.; Kołacz, T.; Lerch, T.; Skwarczyński, J. Measurement Tests and FEM Calculations of DC Excited Flux Switching Motor Prototype. *Energies* **2021**, *14*, 4353. [CrossRef]
2. Caruso, M.; di Tommaso, A.O.; Emma, S.; Miceli, R. Analysis, characterization and minimization of IPMSMs cogging torque with different rotor structures. In Proceedings of the Twelfth International Conference on EVER, Monte Carlo, Monaco, 11–13 April 2017; IEEE Eindhoven University of Technology: Eindhoven, The Netherlands, 2017.
3. Sangdehi, S.M.K.; Abdollahi, S.E.; Gholamian, S.A. Cogging Torque Reduction of 6/13 Hybrid Excited Flux Switching Machine with Rotor Step Skewing. In Proceedings of the 5th Conference on Knowledge Based Engineering and Innovation (KBEI), Tehran, Iran, 28 February–1 March 2019.
4. Ueda, Y.; Takahashi, H. Transverse-Flux Motor Design with Skewed and Unequally Distributed Armature Cores for Reducing Cogging Torque. *IEEE Trans. Magn.* **2017**, *53*, 1–5. [CrossRef]
5. Goryca, Z.; Różowicz, S.; Różowicz, A.; Pakosz, A.; Leśko, M.; Wachta, H. Impact of Selected Methods of Cogging Torque Reduction in Multipolar Permanent-Magnet Machines, a DC motor without magnets or brushes. *Energies* **2020**, *13*, 6108. [CrossRef]
6. Knypiński, Ł.; Nowak, L. The algorithm of multi-objective optimization of PM synchronous motors. *Przegląd Elektrotechniczny* **2019**, *95*, 242–245. [CrossRef]
7. Bernatt, J. *Electrical and Magnetic Circuits of Electrical Machines Excited with Permanent Magnets*; Research and Development Centre of Electrical Machines Komel: Katowice, Poland, 2010.
8. Drabek, T.; Matras, A.; Skwarczyński, J. Simulation of permanent magnet synchronous machine. *Przegląd Elektrotechniczny* **2008**, *84*, 38–41.

9. Anuja, T.A.; Doss, M.A.N. Reduction of Cogging Torque in Surface Mounted Permanent Magnet Brushless DC Motor by Adapting Rotor Magnetic Displacement. *Energies* **2021**, *14*, 2861. [CrossRef]
10. Goryca, Z.; Paduszyński, K.; Pakosz, A. The influence of asymmetrical distribution of rotor's magnets on the cogging torque of the multipolar machine. In Proceedings of the 18th International Symposium on Electromagnetic Fields in Mechatronics, Electrical and Electronic Engineering (ISEF) Book of Abstracts, Lodz, Poland, 14–16 September 2017.
11. Zhu, W.H.X. Cogging Torque Suppression in Flux-Switching Permanent Magnet Machines by Superposition of Single Rotor Tooth. In Proceedings of the IEEE Energy Conversion Congress and Exposition (ECCE), Portland, ON, USA, 23–27 September 2018.
12. Bao, J.; Gysen, B.L.J.; Boynov, K.; Paulides, J.J.H.; Bastiaens, K.; Lomonova, E.A. Analysis and minimization of torque ripple for variable flux reluctance machines. In Proceedings of the IEEE International Electric Machines and Drives Conference (IEMDC), Miami, FL, USA, 21–24 May 2017.
13. García-Gracia, M.; Jiménez, A.R.; Martín, S.A. Cogging Torque Reduction Based on a New Pre-Slot Technique for a Small Wind Generator. *Energies* **2018**, *11*, 3219. [CrossRef]
14. Dobzhanskyi, O.; Gouws, R.; Amiri, E. Optimal switching-flux motor design and its cogging effect reduction. In Proceedings of the IEEE 58th International Scientific Conference on Power and Electrical Engineering of Riga Technical University (RTUCON), Riga, Latvia, 12–13 October 2017.
15. Sulaiman, E.; Romalan, G.M.; Halim, N.A. Skewing and notching configurations for torque pulsation minimization in spoke-type interior permanent magnet motors. In Proceedings of the International Conference on Control, Electronics, Renewable Energy and Communications (ICCEREC), Bandung, Indonesia, 13–15 September 2016.
16. Cui, Y.; Zhang, F.; Huang, L.; Chen, Z. Analysis and Verification of a Cogging Torque Reduction Method for Variable Flux Memory Permanent Magnet Machine. *Electronics* **2021**, *10*, 1913. [CrossRef]
17. Bao, J.; Gysen, B.L.J.; Boynov, K.; Paulides, J.J.H.; Lomonova, E.A. Torque Ripple Reduction for 12-Stator/10-Rotor-Pole Variable Flux Reluctance Machines by Rotor Skewing or Rotor Teeth Non-Uniformity. *IEEE Trans. Magn.* **2017**, *53*, 1–5. [CrossRef]
18. Pompermaier, C.; Washington, J.; Sjöberg, L.; Ahmed, N. Reduction of cogging torque in transverse flux machines by stator and rotor pole shaping. In Proceedings of the IEEE Energy Conversion Congress and Exposition (ECCE), Milwaukee, WI, USA, 18–22 September 2016.
19. Awah, C.C.; Okoro, O.I.; Chikuni, E. Cogging torque and torque ripple analysis of permanent magnet flux-switching machine having two stators. *Arch. Electr. Eng.* **2019**, *68*, 115–133.
20. You, Z.C.; Yang, S.M. Control System for a Single-Phase DC-Excited Flux-Switching Machine with a Torque Ripple Reduction Scheme. *IEEE Access* **2020**, *8*, 226579–226590. [CrossRef]
21. You, Z.C.; Yang, S.M. Modeling Torque Characteristic of Single-Phase DC-Excited Flux Switcing Motor for Torque Ripple Reduction. In Proceedings of the 44th Annual Conference of the IEEE Industrial Electronics Society (IECON), Omni Shoreham, DC, USA, 21–23 October 2018.